Appl. Phys. B (2016) 122:127
DOI 10.1007/s00340-016-6401-4

Applied Physics B
Lasers and Optics

Combined spontaneous Stokes and coherent anti-Stokes Raman scattering spectroscopy

Karina Becker[1] · **Johannes Kiefer**[1,2,3]

Received: 9 February 2016 / Accepted: 24 March 2016 / Published online: 27 April 2016

Abstract The simultaneous determination of multiple parameters is the key in the characterization of processes and materials that change with time. In combustion environments, the combined measurement of temperature and chemical composition is particularly desirable. In the present work, possible approaches for the simultaneous application of spontaneous Raman scattering (RS) and coherent anti-Stokes Raman scattering (CARS) spectroscopy are proposed and analyzed. While RS provides concentration information of all major species, vibrational CARS is a highly accurate thermometry tool at flame conditions. Five experimentally feasible CARS–RS schemes are identified and discussed with respect to signal intensity, measurement volume, and experimental complexity. From this analysis, one scheme was found to be the best option. It utilizes a broadband dye laser centered at 852 nm as a pump and the fundamental 1064-nm radiation of the Nd:YAG as Stokes laser. The third harmonic is used as CARS probe and RS laser. The experimentally most elegant scheme replaces the third harmonic in the above scheme by the second harmonic hence involving the smallest number of optical components in the setup.

Dedicated to Prof. Dr.-Ing. Dr. h.c. Alfred Leipertz on the occasion of his 70th birthday.

✉ Johannes Kiefer
jkiefer@uni-bremen.de

[1] Technische Thermodynamik, Universität Bremen, Badgasteiner Str. 1, 28359 Bremen, Germany

[2] School of Engineering, University of Aberdeen, Aberdeen, UK

[3] Erlangen Graduate School in Advanced Optical Technologies, Universität Erlangen-Nürnberg, Erlangen, Germany

1 Introduction

Over the last 50 years, laser-based diagnostics have transformed combustion science and technology. Laser combustion diagnostics allow non-intrusive measurements of a variety of parameters in a flame or spray with high spatial and temporal resolution [1–5]. For example, the temperature and the concentration of all major species are key quantities to characterize a flame. In order to obtain correlated information, e.g., in a turbulent flame, these parameters need to be determined at the same time. However, to measure them all simultaneously is still a big challenge.

Spontaneous Raman scattering (RS) spectroscopy is a method capable of such multi-parameter measurements [6]. The Raman process is non-resonant, and consequently all Raman-active species contribute their molecular fingerprint to the signal at the same time. Unfortunately, the Raman signal is inherently weak, and thus significant experimental effort is required to achieve data with reasonably good accuracy and precision. This is particularly the case when temperature information is to be derived. Hence, Raman spectroscopy is mainly used for determining the concentration distribution of the major species [7–11]. On the other hand, coherent anti-Stokes Raman scattering (CARS) spectroscopy is a highly sensitive thermometry tool [4, 12, 13], but its potential for multi-species detection is limited. Therefore, most applications of CARS focus on nitrogen thermometry in air-fed combustion systems. Extending this approach to additional species means an additional experimental effort like the use of dual- or triple-pump CARS [14–17], the wide-CARS method [18], or hyperspectral approaches [19].

Combining spontaneous Raman and CARS spectroscopy to overcome the limitations of both methods seems

to be worthwhile. The simultaneous application of pure rotational CARS and Raman has been demonstrated by Weikl et al. [20]. Their aim was to determine the temperature and gas-phase composition during the injection of liquid propane into air. As the process took place at moderately elevated temperature (up to ~350 K), rotational CARS was the method of choice to provide sufficient accuracy. In dual-broadband rotational CARS, two beams from a broadband dye laser serve as pump and Stokes beams to drive rotational Raman coherences for the CARS process, and a third narrowband beam serves as a probe [21, 22]. As the two-photon excitation of rotational Raman transitions is obtained by pulses from the same broadband laser source, its wavelength can be chosen independent of the probe laser. Therefore, Weikl and coworkers arranged their experiment such that the CARS probe beam could serve as Raman excitation source at the same time. In order to avoid spectral interferences from elastically scattered laser light of any of the involved laser beams with the weak Raman signals, the broadband dye laser wavelength was shifted to the near-infrared, and the second harmonic of a Nd:YAG at 532 nm was used as narrowband probe. The resulting Raman spectrum of interest was positioned spectrally in between the laser wavelengths. While the pump and Stokes pulses had energy of about 5 mJ each, the probe pulse energy was cranked up to ~100 mJ to produce appropriate Raman signal intensities.

At higher temperature like in a flame, however, vibrational CARS is typically better suited as it provides a better accuracy and precision under such conditions [23]. Therefore, the combination of vibrational CARS and Raman spectroscopy is desirable. Unfortunately, this application is not as straightforward as in the pure rotational CARS case, where the wavelength of the broadband laser can be chosen arbitrarily.

The aim of the present work is to identify suitable approaches to simultaneous CARS–Raman experiments and to compare them. We limit ourselves to the well-established nanosecond CARS thermometry techniques as the use of ultrashort pulses, which are inherently broadband and typically exhibit relatively low power, are not suitable for Raman spectroscopy in flames. Nanosecond CARS thermometry is usually based on the nitrogen molecule and experimentally realized using a Nd:YAG laser to provide the narrowband beams for CARS, and to pump a dye laser to provide broadband radiation. In the next section, the possible wavelength combinations and pump–probe schemes are presented. Thereafter, these schemes are analyzed with respect to the energy and momentum conservation requirements. This allows estimating the relative signal intensities that can be obtained at the CARS and Raman ends. "Experimental considerations" section discusses experimental implications. "Summary and conclusion" section concludes.

2 Possible approaches

In standard vibrational CARS of nitrogen, the pump and the probe beams are taken from the same laser source, typically the second harmonic of a Nd:YAG laser at 532 nm. Another part of the laser output is used to pump a dye laser to provide broadband Stokes radiation around 607 nm. The frequency difference between 532 and 607 nm matches the vibrational transition of nitrogen (~2330 cm^{-1}), and hence the pump and Stokes pulses can effectively drive vibrational Raman coherences. This approach, however, is not suitable for combined CARS–Raman measurements. Because when the 532-nm radiation also serves as Raman excitation source, the strong elastically scattered light of the broadband Stokes laser will spectrally overlap with the Raman spectrum and affect the measurement. Hence, the combination of laser wavelengths for CARS–RS has to be selected carefully to avoid interferences.

For Raman spectroscopy, a narrowband laser with sufficiently high pulse energy is required. Therefore, any harmonic of the Nd:YAG laser appears suitable. The fundamental beam at 1064 nm would lead to Raman signals in the near-infrared beyond 1 µm and thus cannot be detected with the conventional silicon based detectors. Moreover, the scattering cross section is proportional to λ^{-4}, and therefore 1064-nm excitation would result in very weak signals anyway. At the other end, wavelengths below 300 nm seem desirable because of the high scattering cross section, but require expensive UV optics as the common borosilicate glasses are not transmissive anymore. Also the spectral resolution may be an issue [24]. This leaves the second and third harmonic at 532 and 355 nm, respectively, for generating Raman signals.

As mentioned above, a degenerate two-color CARS scheme is also not possible because of the spectral interferences. Since the frequency difference between the pump and Stokes lasers always has to match the vibrational frequency of nitrogen, the use of the CARS pump laser as the source for Raman scattering is ruled out. Another possible degenerate scheme is to have a broadband pump laser and the same narrowband laser for the Stokes and probe beams. In this case, however, the CARS signal will be at the same wavelength as the pump and may suffer from interferences. Therefore, this option is not considered in the following. The discussed restrictions and boundary conditions lead to five possible schemes. Their energy level diagrams are presented in Fig. 1a–e together with a schematic stick spectrum for each case. A closer look reveals that all schemes make use of the same idea as the work of Weikl et al. [20],

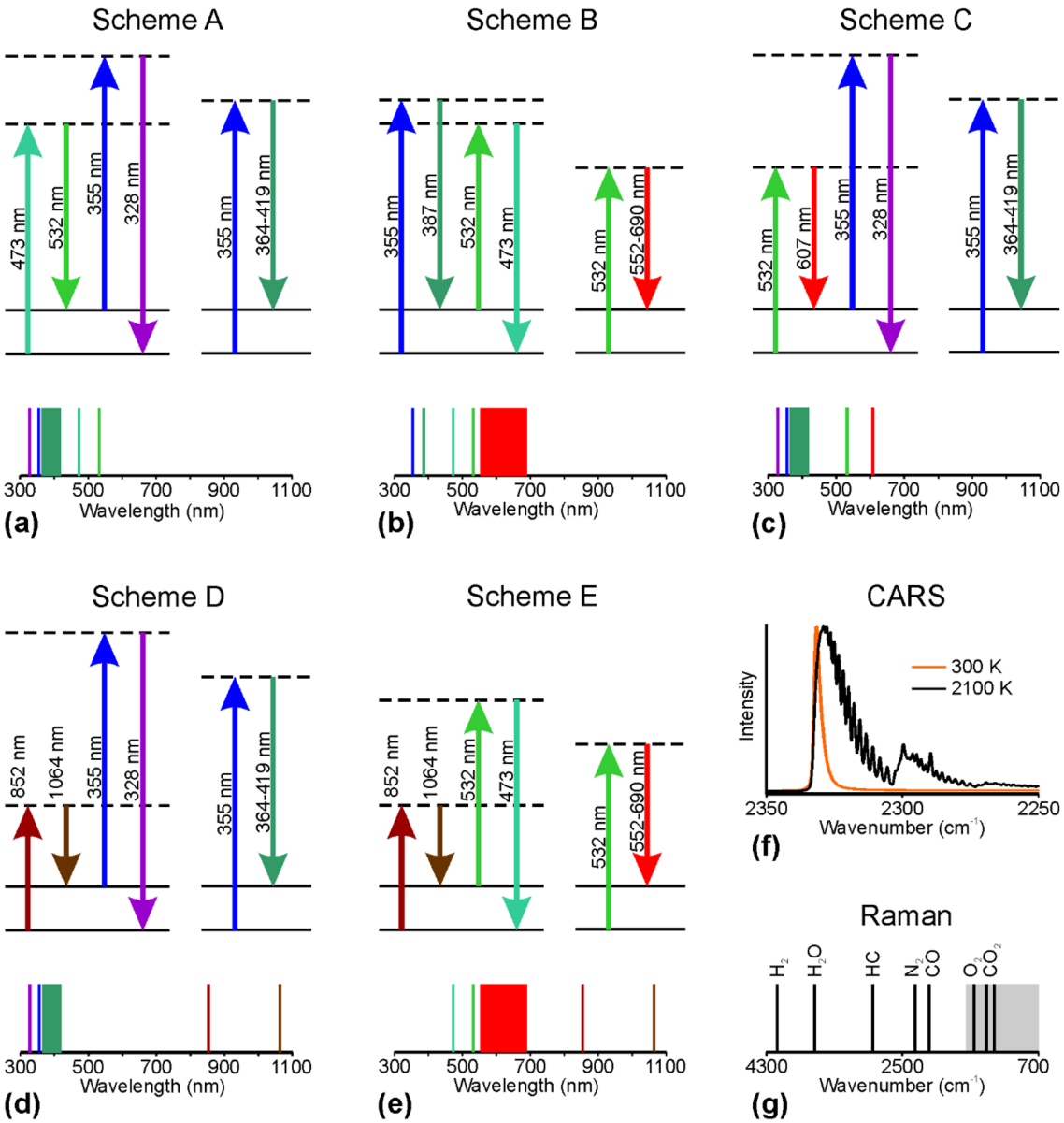

Fig. 1 Energy level diagrams and schematic spectra of the five possible CARS–Raman schemes (**a**–**e**). **f** Simulated CARS spectra of nitrogen. **g** Stick Raman spectrum indicating the positions of the signals of the major species in combustion environments. The *gray area* indicates the fingerprint region

in which the two-photon pumping of the Raman coherences via the pump and Stokes pulses was spectrally separated from the probe and the Raman signal.

Scheme A (Fig. 1a) uses a broadband dye laser beam at 473 nm as a pump and the second harmonic of the Nd:YAG as Stokes laser. The CARS probe and Raman laser is the third harmonic of the Nd:YAG. The stick spectrum below the energy level diagram indicates the ranges of the Raman spectrum and the CARS signal. Further details about the signals are provided schematically in the panels (f) and (g) of Fig. 1. Panel (f) shows theoretical CARS spectra of nitrogen at 300 and 2100 K. The wavenumber range is rather narrow and hence the signal appears as a stick in the schematic spectrum below the energy level diagrams. Panel (g) illustrates a Raman stick spectrum indicating the spectral positions of the typical major species in combustion environments. The gray area indicates the fingerprint region, where most of the hydrocarbon species exhibit characteristic features.

Scheme B utilizes the third harmonic of the Nd:YAG in combination with a broadband dye laser at 387 nm to drive the nitrogen Raman coherences in the CARS process.

The second harmonic serves as a CARS probe and Raman laser. Scheme C uses the Nd:YAG second harmonic and a broadband dye laser at 607 nm as pump and Stokes source, respectively. The CARS probe and Raman excitation is realized with the third harmonic of the Nd:YAG. The schemes D and E both involve the fundamental Nd:YAG radiation at 1064 nm as Stokes pulses and a broadband dye laser at 852 nm serves as the pump. In scheme D the CARS probe and Raman laser is the third harmonic, and in scheme E it is the second harmonic of the Nd:YAG.

All the schemes in Fig. 1 allow simultaneous temperature and multi-species measurements by the combined acquisition of vibrational CARS and Raman signals. However, identifying the best scheme for a given application is not straightforward though. Hence, the next section will analyze the schemes more in detail.

3 Analysis of approaches

As aforesaid, the Raman process is non-resonant, and thus a laser with an arbitrary wavelength can be used, in principle. Being a four-wave mixing method, CARS involves more complicated physics, and the signal generation requires that energy and momentum of the four waves involved in the interaction are conserved. The energy conservation leads to the wavelength selection for each scheme as shown in the previous section. The momentum conservation has implications for the geometry, in which the beams are all overlapping to ensure the generation of a coherent signal. Both requirements influence the signal intensity that can be expected, and hence this section will analyze the different schemes in this respect.

3.1 Energy conservation

The selected wavelengths have implications for the signal intensity mainly because the scattering cross section is strongly wavelength depended. The full equation of the CARS and Raman signal intensities can be found in the literature, see e.g., [5, 25]. For the comparison of the different schemes in the present work, however, we do not take the full equations into account but use a simplified approach by considering the scattering cross sections only. The wavenumber dependence of Stokes and anti-Stokes Raman processes can be described as

$$\left(\frac{\partial\sigma}{\partial\Omega}\right)_{\text{Stokes}} \propto (\nu_0 - \nu_R)^4 \tag{1a}$$

$$\left(\frac{\partial\sigma}{\partial\Omega}\right)_{\text{anti-Stokes}} \propto (\nu_0 + \nu_R)^4 \tag{1b}$$

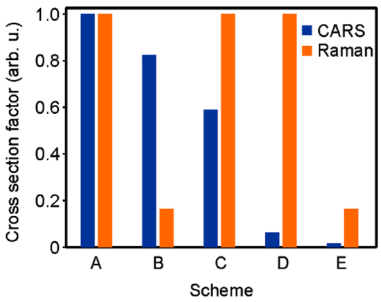

Fig. 2 Intensity variations that can be expected due to the wavenumber dependences of the Raman scattering cross section

where $(\partial\sigma / \partial\Omega)$ is the differential scattering cross section, ν_0 is the wavenumber of the incident radiation (the laser in our case), and ν_R is the wavenumber of the Raman transition, which is often referred to as the Raman shift. On the Raman side, we consider a spontaneous Stokes process and hence we can estimate the changes of the intensity for the different schemes by simply calculating the $(\nu_{\text{probe}} - \nu_R)^4$ factors. Assuming that the Raman laser intensities and the dimensions of the measurement volume are the same for every scheme, the resulting factors give an estimate of the expected signal intensities. As there are only two different excitation wavelengths viz. the second and third harmonic Nd:YAG radiation, there are only two signal levels, which are plotted in Fig. 2 normalized with respect to the value of the third harmonic.

In CARS, the wavelength dependence is more complicated given the nonlinear nature of the process. However, we simplify this by splitting the four-wave mixing into a stimulated Stokes Raman pumping process and an anti-Stokes scattering. The wavenumber dependence of this simplistic model can then be described by the product $(\nu_{\text{pump}} - \nu_R)^4 \cdot (\nu_{\text{probe}} + \nu_R)^4$. For completeness, we note that this model was checked against the full CARS signal equation, and it was found that it delivered the same trends between the setups. The resulting values normalized with respect to the maximum are plotted in Fig. 2. The highest intensity can be expected for scheme A. This shows that the wavelength of the probe laser is important here as it determines the anti-Stokes wavelength of the signal and hence the dominating factor of the product. The effect of exchanging the pump and probe can be seen from the results for the schemes B and C. The schemes D and E exhibit the smallest signal intensities. This is reasonable as they involve near-infrared lasers to deliver the pump and Stokes pulses.

From the analysis of the wavelength-dependent scattering cross sections, the schemes A, B, and C seem to be most suited from a CARS point of view. The Raman signals are strongest in schemes A, C, and D, since 355-nm

excitation is used. As scheme A provides the highest values for both techniques simply because it provides the largest Stokes wavelength ($\nu_{\text{pump}} - \nu_R$), it seems to be the best option at this point.

3.2 Momentum conservation

In CARS, the geometric configuration of the beam overlap is crucial. In a quantum mechanical sense, it requires that the momentum of all four photons involved in the interaction is conserved. In a wave sense, this means that the phases have to be matched in order to obtain a coherent superposition. The corresponding wave vector diagram using the example of scheme C is shown in Fig. 3a. When the wave vectors form a closed tetragon, the phase mismatch is zero and the signal intensity is maximized. For the experimentalist, this means that the angles, at which the beams cross, are the crucial parameters. In the laboratory practice, it is common to align a CARS setup such that the three laser beams are guided parallel to each other and then focused into the measurement volume by the same lens as shown in Fig. 3b. Assuming an achromatic lens, the angles can easily be set by the positions of the incident beams on the lens and their distance from the lens center. In this way, a multitude of phase-matching geometries can be realized including the common planar and folded BOXCARS arrangements [5, 26]. The beam geometry in the focal spot eventually determines the shape of the measurement volume [27], and influences the signal intensity. For a simplistic collinear configuration, it can be shown that the signal intensity is proportional to the square of the length of the measurement volume [5]. Strictly speaking, this relationship only holds for collinear plane wavefronts, while we will consider focused beams in this work. However, it is reasonable to assume that the wavefronts in the focal waist of a Gaussian beam are plane over a small distance. In addition, the crossing angles of the beams with respect to the optical axis are considered small. Hence, the assumption of a quadratic relationship is justified in the semiquantitative assessment to be presented in the following.

In order to compare the five different CARS-RS schemes, we consider a planar BOXCARS geometry as shown in Fig. 3b. Even this configuration leaves a high degree of freedom in an experiment. Herein, a single case with the following parameters will be examined: (1) The lens is achromatic and has a focal length of 300 mm; (2) The beams are Gaussian beams and have a diameter of 10 mm before the lens; (3) The pump beam is located at a distance of $x_{\text{pump}} = 15$ mm from the optical axis. These boundary conditions determine all the angles and distances. The CARS measurement volume geometry, in particular its length, can then be determined by looking at the region where all three laser beams overlap. This overlap has been simulated and a 2D projection of such an overlap is shown in Fig. 3c. The plot shows the beam waist in the vicinity of the focal spot without taking the intensity distribution into account. As the beams have different wavelengths, the

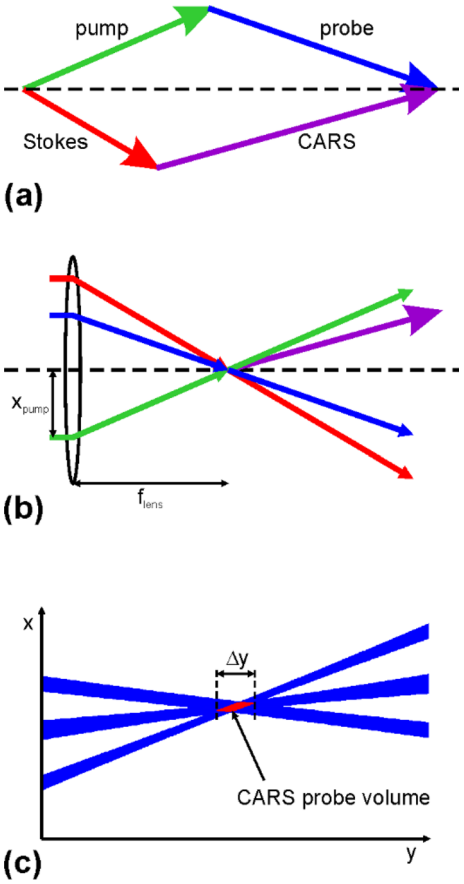

Fig. 3 **a** CARS wave vector diagram. **b** Schematic arrangement to obtain phase-matching conditions in CARS. **c** 2D projection of the beam overlap in CARS; the *red area* illustrates the measurement volume

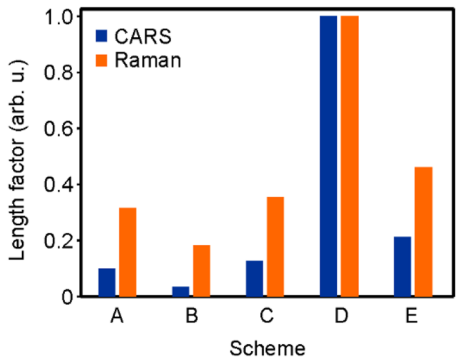

Fig. 4 Intensity variations that can be expected due to the dependences on the measurement volume length

resulting waists in the focal plane exhibit different diameters. The red area represents the region, in which all three beams are present.

For further analysis, the measurement volume length was determined as the distance Δy that ranges between the two ends of the red area on the y-axis. Like for the scattering cross section, a simple factor is used to estimate the influence of the measurement volume length on the signal intensity. As mentioned above, in CARS the signal intensity depends on the squared length, whereas the RS signal is known to be linear versus probe volume length. Normalizing the resulting values with respect to the maximum, which is found for scheme D, the distribution shown in Fig. 4 is obtained. Scheme D exhibits the longest volume, the volumes of the schemes A, C, and E are about 50–70 % shorter, and that of scheme B is about 80 % shorter. The length factors plotted in Fig. 4 vary accordingly.

The Raman measurement volume can be treated in a much more straightforward manner. Since the Raman process occurs spontaneously, Raman signal is generated as the laser beam propagates through the medium. The measurement volume is determined by the optical components and their arrangement in the signal collection path. Considering the ideal case, i.e., the CARS and Raman measurement volumes should exhibit the same length and should be at the same position, we take the determined length of the CARS volume as Raman volume length. The resulting normalized values are given in Fig. 4. They show the same trend but differ as the Raman signal is a linear function of the measurement volume length.

Note, that the long measurement volume of scheme D is an advantage and a disadvantage at the same time. On the one hand, it ensures strong signals, but, on the other hand, this may mean a poor spatial resolution in an experiment. In a flame environment, a large measurement volume can result in spatial averaging effects that occur when part of the probed gas is hot and another part is cold [28]. This can be the case, when measurements are performed in the vicinity of the flame front, where steep gradients occur thus requiring the best spatial resolution that can be achieved.

3.3 Overall effects

Combining the factors discussed in the preceding subsections means to multiply them for the individual schemes. Normalization of the resulting numbers leads to the intensity factor plotted in Fig. 5. On the CARS side, scheme A offers the highest intensity and the third highest for Raman. The ranks swap in scheme D. Scheme C exhibits the second highest intensity factors for both methods and therefore it seems to be a good compromise at first glance. However, in scheme D the Raman signal is about the threefold, while the CARS signal is only reduced by ~35 % compared to the max value. Therefore, scheme D is rather attractive. In the schemes B and E, both the Raman and the CARS signals are comparatively low. A disadvantage of scheme D is the long measurement volume, which means a reduced spatial resolution.

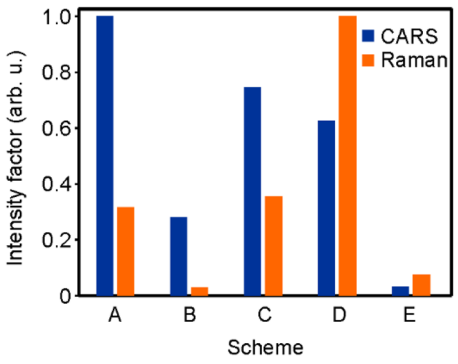

Fig. 5 Intensity variations that can be expected for the different schemes considering scattering cross sections and geometrical aspects

From this analysis, the order of attractiveness in terms of signal intensity is D > C > A > B, E. In the next section, the different schemes will be discussed from an experimental point of view.

4 Experimental considerations

Figure 6 illustrates schematic experimental setups for all the schemes. They are all based on a Nd:YAG laser and a dye laser. The weak Raman signals are detected in direction perpendicular to the laser beam propagation. As the Raman signal is emitted isotropically into a 4π sphere, a fraction of it is collected and collimated by a lens, spectrally filtered, e.g., to reduce elastically scattered light, focused onto the slit of a spectrograph and finally detected with an intensified CCD camera. This general arrangement is well established for the combined use of linear and nonlinear optical methods, for example, when laser-induced fluorescence is combined with degenerate four-wave mixing [29–40], polarization spectroscopy [41–43], laser-induced thermal grating spectroscopy [44], two-color four-wave mixing [45] and six-wave mixing [46], and the earlier simultaneous rotational CARS and Raman technique [20].

In scheme A, the second and third harmonic radiations are required. After the appropriate optical units (polarization optics and nonlinear crystals), the different harmonics are separated using a set of dichroic mirrors. Part of the 355-nm radiation is used to pump the dye laser in order to deliver the 473-nm broadband beam. A suitable dye would be Coumarin 102 dissolved in ethanol. The pump, Stokes, and probe beams for the CARS process are directed to an

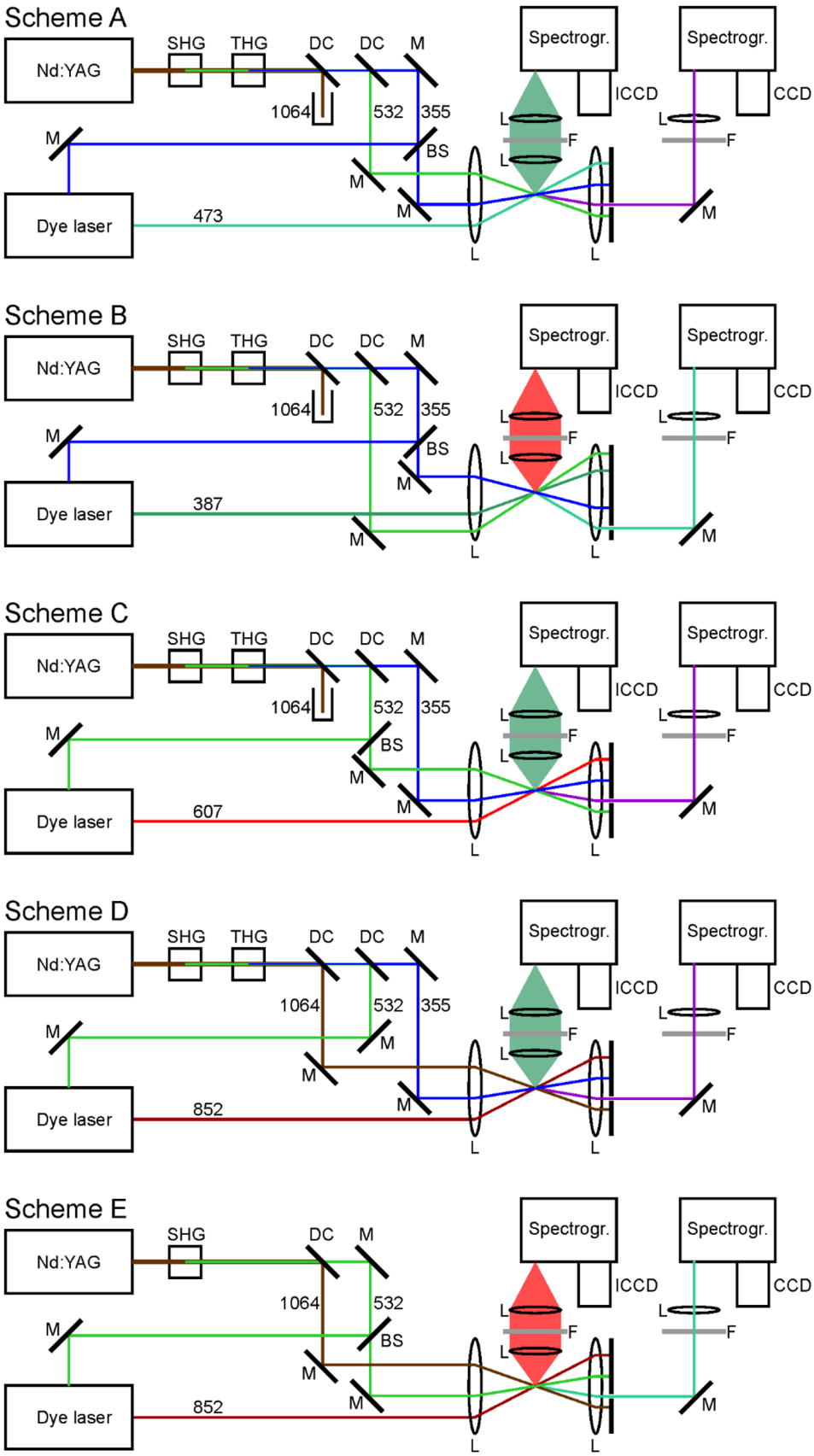

Fig. 6 Possible experimental arrangements for the different CARS–Raman schemes. *SHG* second harmonic generation; *THG* third harmonic generation; *DC* dichroic mirror; *M* mirror; *BS* beam splitter; *L* lens; *F* filter; *ICCD* intensified charge-coupled device camera; *CCD* charge-coupled device camera

achromatic lens and focused into the measurement volume. The Raman signal is collected and detected as described above. The coherent CARS signal is guided to another spectrograph equipped with a CCD camera.

Scheme B is very similar. The dye laser is again pumped by part of the third harmonic of the Nd:YAG and operates at 387 nm, for example, using Exalite 389 dye in p-dioxane. In scheme C, part of the second harmonic is used to pump the dye laser, which then emits radiation at 607 nm. Rhodamine 610 dissolved in ethanol would be a suitable medium for this purpose.

Schemes D and E use near-infrared radiation as pump and Stokes pulses. The Stokes beam is the residual of the fundamental Nd:YAG, while the pump beam at 852 nm is provided by the dye laser. This wavelength can be obtained by pumping LDS 867 dye in methanol with the second harmonic radiation of the Nd:YAG.

From the signal intensity analysis in the previous section the order D > C > A > B, E of the schemes was found. Looking at the experimental setup, however, the scheme E becomes very attractive, as it is the most elegant option. It does not require a third harmonic generation unit and it makes use of the residual 1064 nm radiation that is left after the second harmonic generation. An experimental disadvantage is the generally low conversion efficiency of near-infrared dye, which is typically in the order of 5–10 % according to the specifications provided by the main suppliers. On the other hand, most Nd:YAG lasers provide rather high energy pulses, and hence there is sufficient energy available to pump the dye laser and generate appropriate levels of pulse energy in the near-infrared to drive the CARS process.

Overall, the scheme D still appears to be the best option. It came out top in the signal intensity analysis as it provides the strongest Raman signal and comparatively high CARS signal levels. Looking at the experimental arrangement, it has the disadvantage of requiring a third harmonic generation unit, but the setup is relatively simple as none of the beams has to be split, which would reduce the flexibility of the setup. The entire 1064-nm residual and 852-nm dye laser beams are used as pump and Stokes lasers in the CARS process. The entire third harmonic radiation serves as CARS probe and Raman laser, and the entire second harmonic radiation is used to pump the dye laser. A possible problem using 355 nm as Raman laser, however, may arise in rich flames where strong fluorescence interferences from polycyclic aromatic hydrocarbons (PAH) may obscure the weak Raman signals. A polarization-resolved detection can be a solution, but it requires a second spectrograph and camera at the Raman end [9]. Hence, it adds experimental complexity. Scheme E, which employs the 532-nm wavelength, will avoid or at least reduce this problem on the Raman side, but then the CARS signal will occur around 473 nm, which may cause interference with chemiluminescence of C_2 radicals [47]. Finally, as already mentioned, near the flame front, the spatial resolution of E will be an advantage as regards to the D arrangement.

5 Summary and conclusion

In the present work, the possible schemes for combining vibrational Raman and vibrational CARS spectroscopy were analyzed and compared. The combination of the two methods has the potential for simultaneous temperature and multi-species measurements in flame environments, but to find the best combination of lasers and an optimal experimental setup is not straightforward.

Employing the common Nd:YAG laser, five different schemes have been identified. An analysis to estimate the variations in the expected signal levels and measurement volume lengths was followed by a discussion of possible experimental setups for the individual schemes. From this analysis, one scheme was found to be the best option. It utilizes a broadband dye laser centered at 852 nm as a pump and the fundamental 1064-nm radiation of the Nd:YAG as Stokes laser. The third harmonic is used as CARS probe and Raman laser. A minor disadvantage of this scheme is the relatively long measurement volume. However, this can easily be reduced by choosing a different experimental geometry such as a folded BOXCARS arrangement. The experimentally most elegant scheme replaces the third harmonic in the above scheme by the second harmonic. It takes a reduction in signal intensity, but at the benefit of involving the smallest number of optical components in the setup and of a better spatial resolution.

References

1. M. Aldén, J. Bood, Z.S. Li, M. Richter, Proc. Combust. Inst. **33**, 69–97 (2011)
2. T.D. Fansler, S.E. Parrish, Meas. Sci. Technol. **26**, 012002 (2015)
3. J. Kiefer, P. Ewart, Prog. Energy Combust. Sci. **37**, 525–564 (2011)
4. S. Roy, J.R. Gord, A.K. Patnaik, Prog. Energy Combust. Sci. **36**, 280–306 (2010)
5. A.C. Eckbreth, *Laser Diagnostics for Combustion Temperature and Species*, 2nd ed. (Gordon and Breach, Amsterdam, 1996)
6. O. Keck, W. Meier, W. Stricker, M. Aigner, Combust. Sci. Technol. **174**, 117–151 (2002)
7. W. Meier, R.S. Barlow, Y.L. Chen, J.Y. Chen, Combust. Flame **123**, 326–343 (2000)
8. C. Dreyer, T. Parker, M.A. Linne, Appl. Phys. B **79**, 121–130 (2004)
9. J. Egermann, T. Seeger, A. Leipertz, Appl. Opt. **43**, 5564–5574 (2004)
10. R.S. Barlow, S. Meares, G. Magnotti, H. Cutcher, A.R. Masri, Combust. Flame **162**, 3516–3540 (2015)

11. T. Seeger, J. Egermann, S. Dankers, F. Beyrau, A. Leipertz, Chem. Eng. Technol. **27**, 1150–1156 (2004)
12. F. Vestin, M. Afzelius, H. Berger, F. Chaussard, R. Saint-Loup, P.-E. Bengtsson, J. Raman Spectrosc. **38**, 963–968 (2007)
13. C.J. Kliewer, Y. Gao, T. Seeger, J. Kiefer, B.D. Patterson, T.B. Settersten, Proc. Combust. Inst. **33**, 831–838 (2011)
14. R.P. Lucht, Opt. Lett. **12**, 78–80 (1987)
15. S. Roy, T.R. Meyer, M.S. Brown, V.N. Velur, R.P. Lucht, J.R. Gord, Opt. Commun. **224**, 131–137 (2003)
16. F. Beyrau, A. Datta, T. Seeger, A. Leipertz, J. Raman Spectrosc. **33**, 919–924 (2002)
17. M.C. Weikl, Y. Cong, T. Seeger, A. Leipertz, Appl. Opt. **48**, B43–B50 (2009)
18. S.A. Tedder, J.L. Wheeler, A.D. Cutler, P.M. Danehy, Appl. Opt. **49**, 1305–1313 (2010)
19. A. Bohlin, C.J. Kliewer, Appl. Phys. Lett. **105**, 161111 (2014)
20. M.C. Weikl, F. Beyrau, J. Kiefer, T. Seeger, A. Leipertz, Opt. Lett. **31**, 1908–1910 (2006)
21. A.C. Eckbreth, T.J. Anderson, Opt. Lett. **11**, 469–498 (1986)
22. M. Aldén, P.-E. Bengtsson, H. Edner, Appl. Opt. **25**, 4493–4500 (1986)
23. T. Seeger, A. Leipertz, Appl. Opt. **35**, 2665–2671 (1996)
24. J. Kiefer, Appl. Spectrosc. **64**, 687–689 (2010)
25. D.A. Long, *Raman Spectroscopy* (McGraw—Hill International Book Company, London, 1977)
26. J.A. Shirley, R.J. Hall, A.C. Eckbreth, Opt. Lett. **5**, 380–382 (1980)
27. S.A. Tedder, M.C. Weikl, T. Seeger, A. Leipertz, Appl. Opt. **47**, 6601–6605 (2008)
28. T. Seeger, M.C. Weikl, F. Beyrau, A. Leipertz, J. Raman Spectrosc. **37**, 641–646 (2006)
29. P.M. Danehy, R.L. Farrow, JOSA B **13**, 1412–1418 (1996)
30. S. Williams, D.S. Green, S. Sethuraman, R.N. Zare, J. Am. Chem. Soc. **114**, 9122–9130 (1992)
31. P.M. Danehy, E.J. Friedman-Hill, R.P. Lucht, R.L. Farrow, Appl. Phys. B **57**, 243–248 (1993)
32. A.P. Smith, A.G. Astill, Appl. Phys. B **58**, 459–466 (1994)
33. F. Grisch, A. Bresson, P. Bouchardy, B. Attal-Trétout, Aerosp. Sci. Technol. **6**, 465–479 (2002)
34. F. Grisch, B. Attal-Trétout, A. Bresson, P. Bouchardy, V.R. Katta, W.M. Roquemore, Combust. Flame **139**, 23–38 (2004)
35. M. Tulej, G. Knopp, P. Beaud, T. Gerber, P.P. Radi, J. Raman Spectrosc. **36**, 109–115 (2005)
36. S. Kröll, C. Löfström, M. Aldén, Appl. Spectrosc. **47**, 1620–1622 (1993)
37. M. Motzkus, S. Pedersen, A.H. Zewail, J. Phys. Chem. **100**, 5620–5633 (1996)
38. B.A. Mann, R.F. White, R.J.S. Morrison, Appl. Opt. **35**, 475–481 (1996)
39. A. Okazaki, T. Ebata, N. Mikami, J. Chem. Phys. **107**, 8752–8758 (1997)
40. K. Morishita, N. Kawaguchi, T. Okada, Jpn. J. Appl. Phys. **40**, 5326–5328 (2001)
41. Z.T. Alwahabi, J. Zetterberg, Z.S. Li, M. Aldén, Eur. Phys. J. D **42**, 41–47 (2007)
42. J. Kiefer, Z.S. Li, J. Zetterberg, M. Linvin, M. Aldén, Opt. Commun. **270**, 347–352 (2007)
43. J. Kiefer, A. Meyerhoefer, T. Seeger, A. Leipertz, Z.S. Li, M. Aldén, J. Raman Spectrosc. **40**, 828–835 (2009)
44. P.M. Danehy, P.H. Paul, R.L. Farrow, JOSA B **12**, 1564–1576 (1995)
45. M. Tulej, M. Meisinger, G. Knopp, A.M. Walser, T. Gerber, P.P. Radi, J. Raman Spectrosc. **38**, 1022–1031 (2007)
46. W.D. Kulatilaka, R.P. Lucht, S. Roy, J.R. Gord, T.B. Settersten, Appl. Opt. **49**, 3921–3927 (2007)
47. A. Malarski, F. Beyrau, A. Leipertz, J. Raman Spectrosc. **36**, 102–108 (2005)